Atmospheric
Chemistry
and Physics

Supplement of
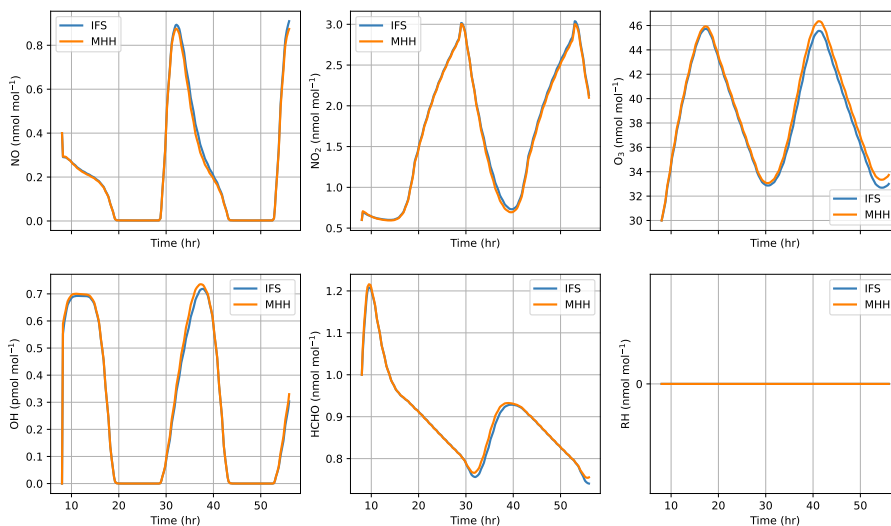
Evaluating NO$_x$ stack plume emissions using a high-resolution atmospheric chemistry model and satellite-derived NO$_2$ columns

Maarten Krol et al.

Correspondence to: Maarten Krol (maarten.krol@wur.nl)

ERH =   0.0, ENO =   0.1 ppb m/s

Figure S1. Box model comparison (h = 1000 m) of the IFS scheme with the condensed MicroHH (MHH) scheme. Results of a two day simulation are shown, starting at 8 AM. Emission strengths of NO and C_3H_6 are given in the figure title. Time series are plotted for NO, NO_2, O_3, OH, HCHO, and RH (C_3H_6).

Box model evaluation of the chemistry scheme

We evaluated the uncertainties associated with the chemistry scheme using a box model. We simulated the chemistry of the full IFS chemistry scheme (IFS) and our simplified version presented in the paper (MHH). The box model considers emissions of NO and hydrocarbons (RH = C_3H_6) at the surface of a 1000 m well-mixed atmospheric box. Diurnal variations in light conditions are accounted for and simulations were run for two days. Figures S1– S9 show the results with varying emission strengths, covering both ozone depletion and ozone production regimes. These regimes are expected in our plume simulations. Like mentioned in the original manuscript, results are almost identical when no emissions of hydrocarbons are considered (ERH = 0). Results deteriorate when emissions of hydrocarbons are considered, but remain acceptable (errors smaller than 10% for NO_2) specifically for NO_2 (sampled by TROPOMI) and when only the first day is considered. Here we note that air masses stay relatively short in our domain and that air masses forced by the CAMS boundary conditions that enter the domain.

Effects of the resolution on plume mixing and chemistry

We also evaluated the effects of resolution on mixing and chemistry in the plume. These results have been obtained with a controlled LES setup with a prescribed west–east wind (10 m s^{-1} geostrophic wind) and prescribed boundary conditions for temperature and chemical species. The simulation domain size was [$\Delta x, \Delta y, \Delta z$] = [9600 m, 4800 m, 3200 m], i.e. much

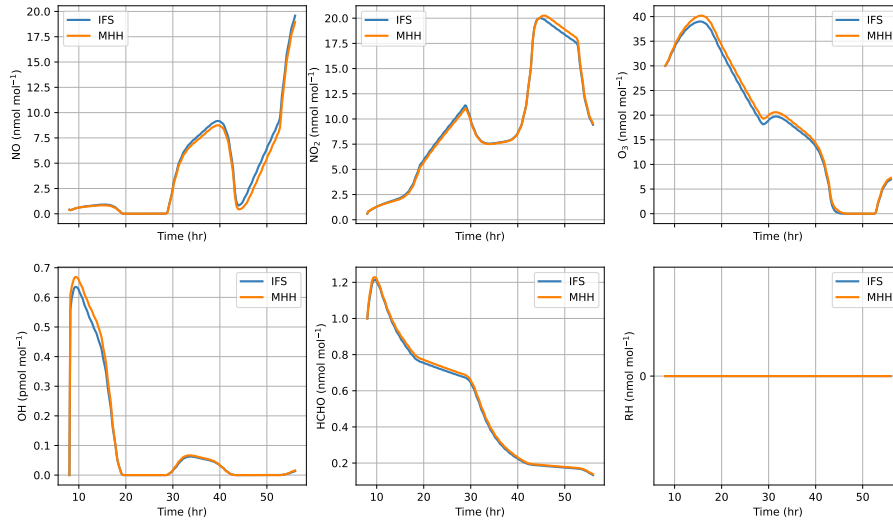ERH =   0.0, ENO =   0.3 ppb m/s

Figure S2. As Figure S1.
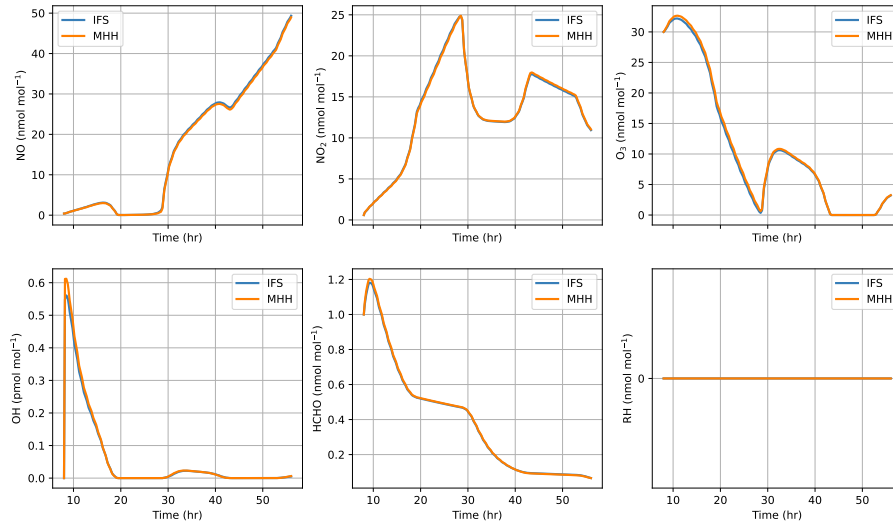
ERH =   0.0, ENO =   0.5 ppb m/s

Figure S3. As Figure S1.

15 smaller compared to the simulation domain in the main paper. These simulations have been performed on different resolutions (200, 100, 50, 25 m) to test the effects of resolution on the main findings. The simulations were forced with a surface heat flux of $0.1\ \mathrm{K\ m\ s^{-1}}$ and emissions from a 200-m high stack, located 1600 m from the west border. The source magnitude was 50%
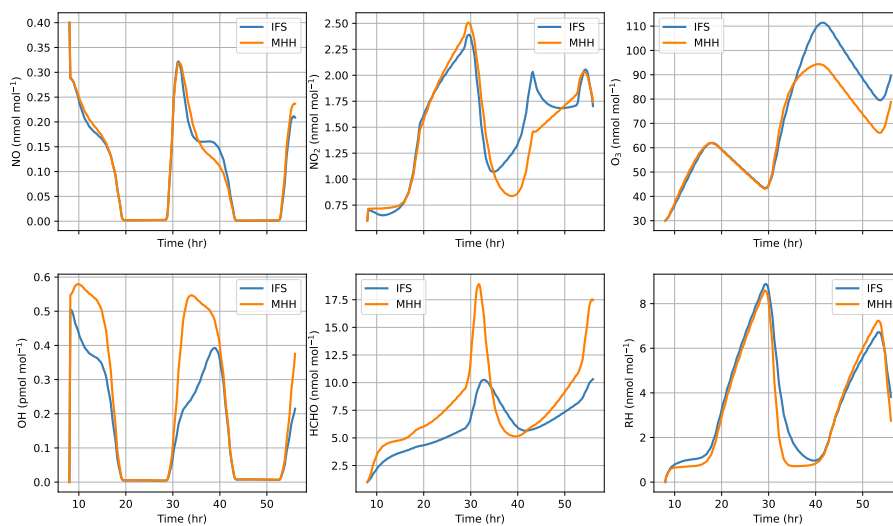
ERH = 0.3, ENO = 0.1 ppb m/s

Figure S4. As Figure S1.

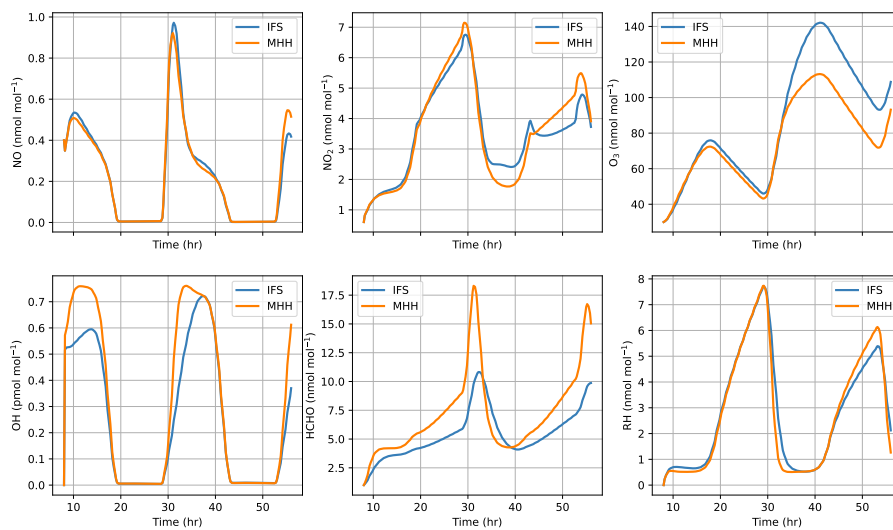ERH = 0.3, ENO = 0.3 ppb m/s

Figure S5. As Figure S1.This figure corresponds to Figure 1 in the main paper.

of the MAT emissions. The simulations were performed for 4 hours (starting at 6 am) and the results were averaged over the last hour of the simulation.
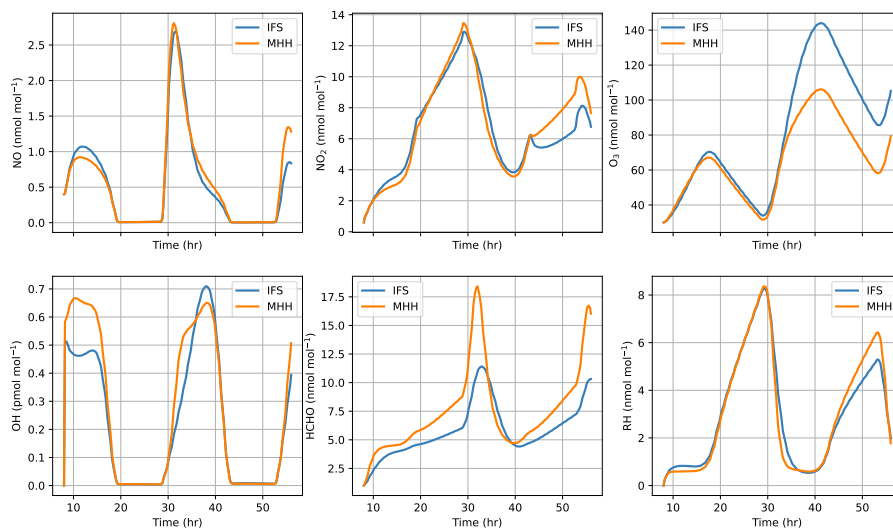
ERH = 0.3, ENO = 0.5 ppb m/s

Figure S6. As Figure S1.
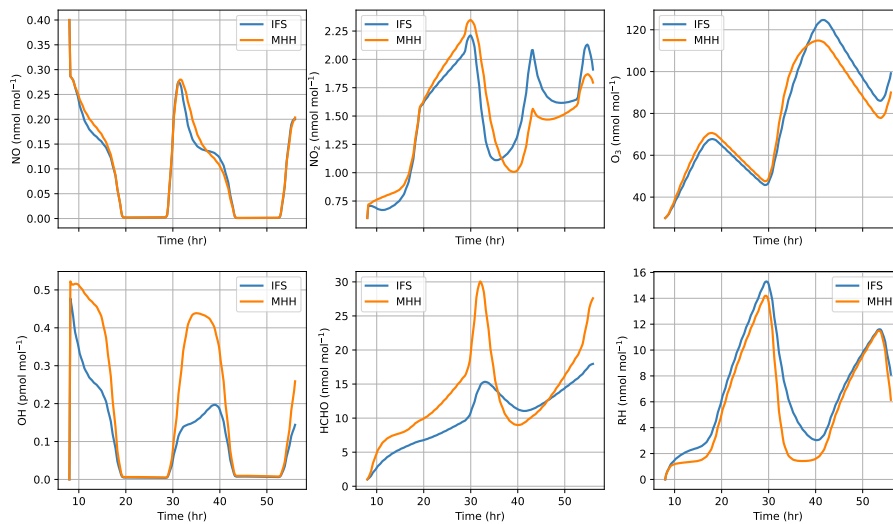
ERH = 0.5, ENO = 0.1 ppb m/s

Figure S7. As Figure S1.

20 First, Figure S10 shows the NO_2 column averaged over the last hour of the simulation. Although the plumes appear similar at different resolutions, the conversion of NO to NO_2 proceeds slower at a finer resolution. This is corroborated in Figures S11, S12, and S13, which show the y-mean columns of, respectively, NO_2, NO, and O_3. Due to emission, sharp concentration

5

ERH =   0.5, ENO =   0.3 ppb m/s
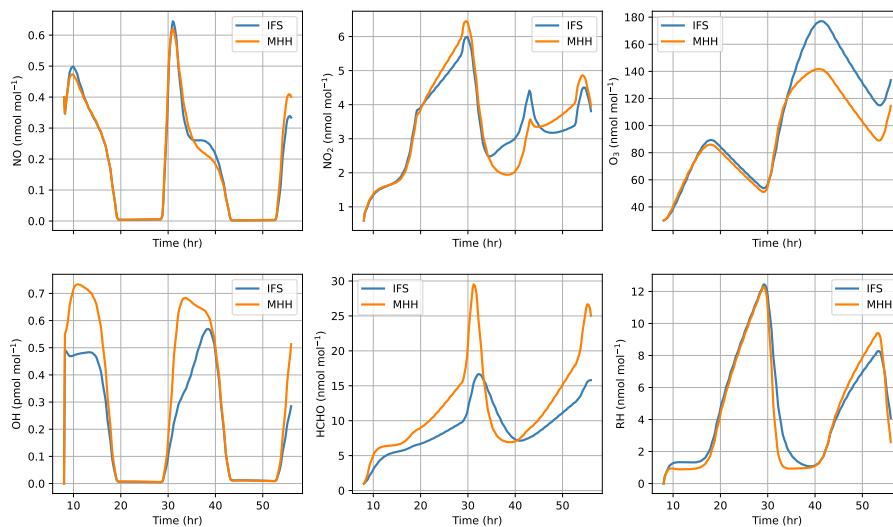

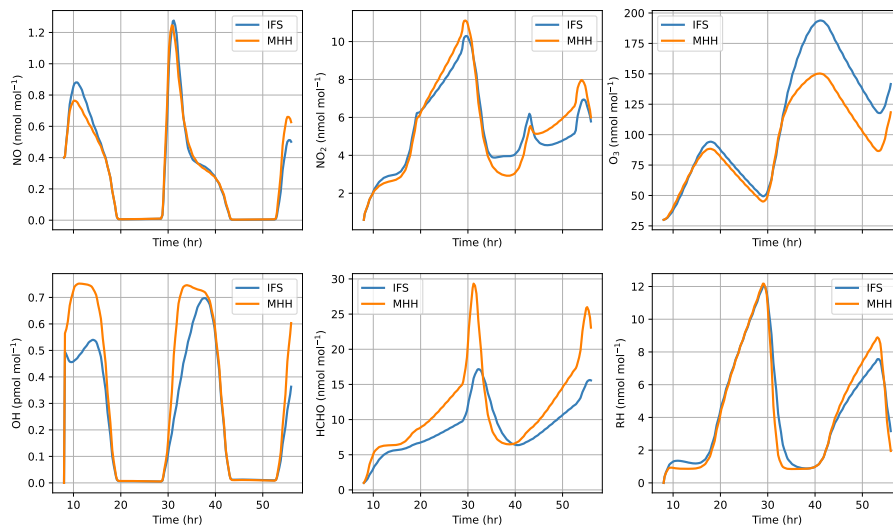**Figure S8.** As Figure S1.

ERH =   0.5, ENO =   0.5 ppb m/s

Figure S9. As Figure S1.

gradients form at the stack location, because O_3 levels are titrated by the high supply of NO. Note that 95% of the NO_x emission
is emitted as NO. These sharp gradients are expected to be resolved better in the high-resolution simulation. Results seem to
converge at a resolution of 25 m. At a resolution of 100 m, as used in the simulations presented in the paper, a substantial instant

25

dilution error is still present. For instance, at a distance of 6000 m from the stack, y-mean NO_2 columns are $\approx$20% larger at 100 m resolution, compared to the 25 m resolution simulation. These errors are hard to avoid if you want to address a larger domain of 50–100 km because the calculation time quickly becomes prohibitive. The 100 m resolution used in the simulations presented in the paper is therefore a compromise, and this issue clearly warrants additional investigation. Concerning the ratio

30 NO_x to NO_2 discussed in the paper, the effect of resolution is also important. Figure S14 shows the calculated ratio downwind of the stack. Although the NO_x to NO_2 ratio shows a clear spike at the emission point, this spike is smaller at 100 m and 200 m resolutions, and the ratio returns faster to background values.

In conclusion, at higher spatial model resolution, the conversion of NO to NO_2 is expected to proceed slower, and the ratios of NO_x to NO_2 are expected to be substantially larger at distances up to 10 km downwind of the stack. These effects likely

35 depend on the emission strength, the background ozone concentration, the wind speed, and the stability of the boundary layer, and warrant further investigation.

Analysis of plume metrics on TROPOMI resulution

Figures S15, S16, S17 and S18 show results for the lifetime of NO_2, the lifetime of NO_x, $I_{s,NO_2,OH}$ and the NO_x to NO_2 ratio, respectively, coarsened to TROPOMI resolution. Note that for the MAT case, the lifetime of NO_2 in the background gets very

40 long, due to depletion of NO_x by oxidation in the extensive domain. As mentioned in the main paper, we focused on emission of a single stack, and added no surface emissions of e.g. traffic. Note also that these figures confirm the finding in the paper that the BEL1, MAT1, and MAT2 plumes remain chemically intact for larger downwind distances.
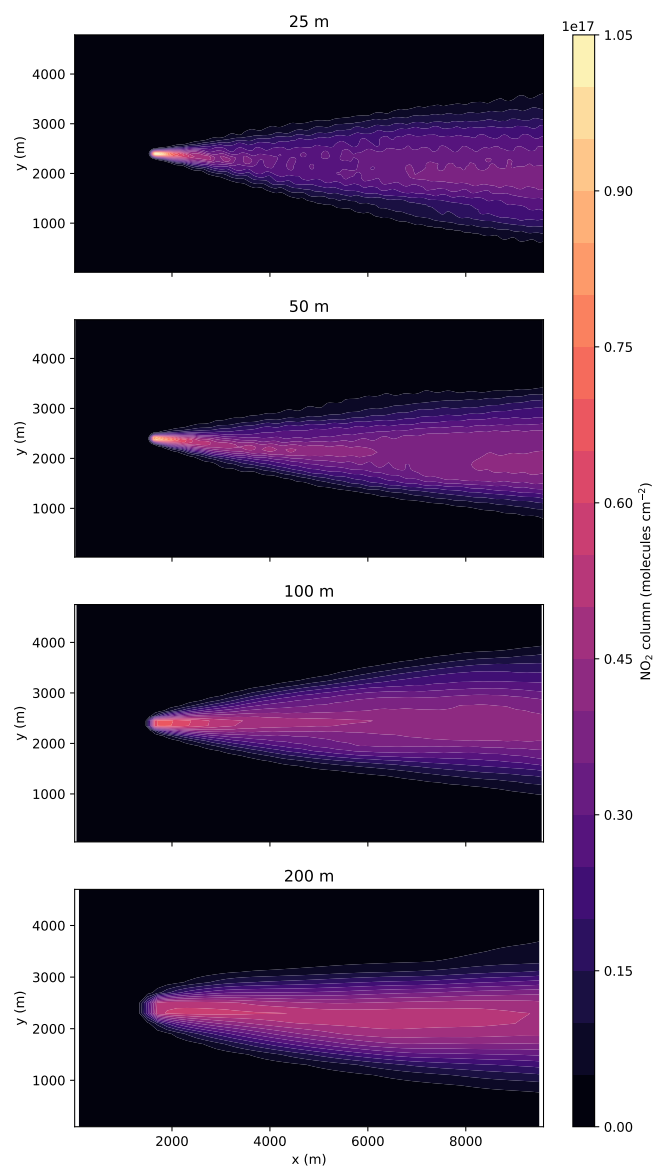
Figure S10. Total column NO_2 averaged over the last hour of a 4 hour simulation on a small domain. Emission with a source strength of half the MAT emissions were added at [x,y,z] = [1600 m, 2400 m, 200 m]. Simulations were performed on resolutions of 25 m (top panel), 50 m, 100 m, and 200 m (bottom panel).
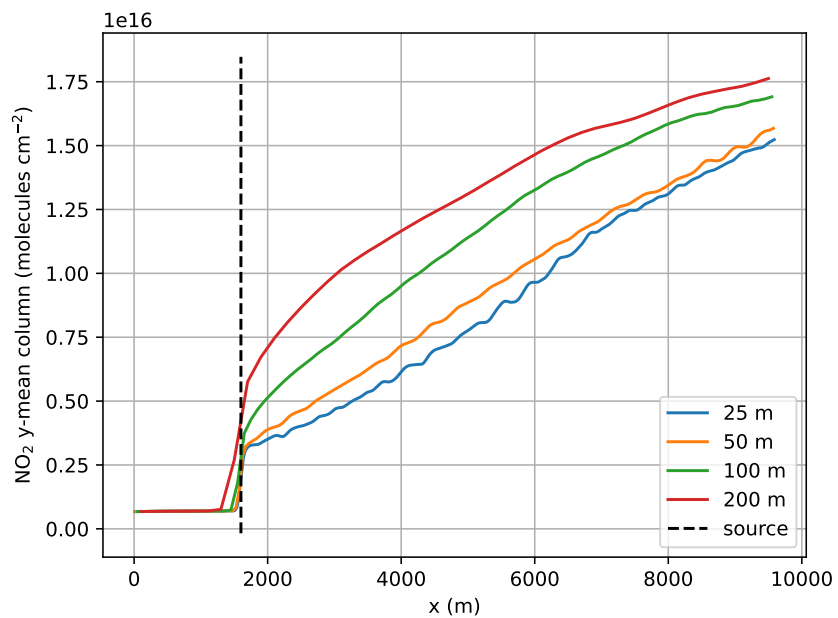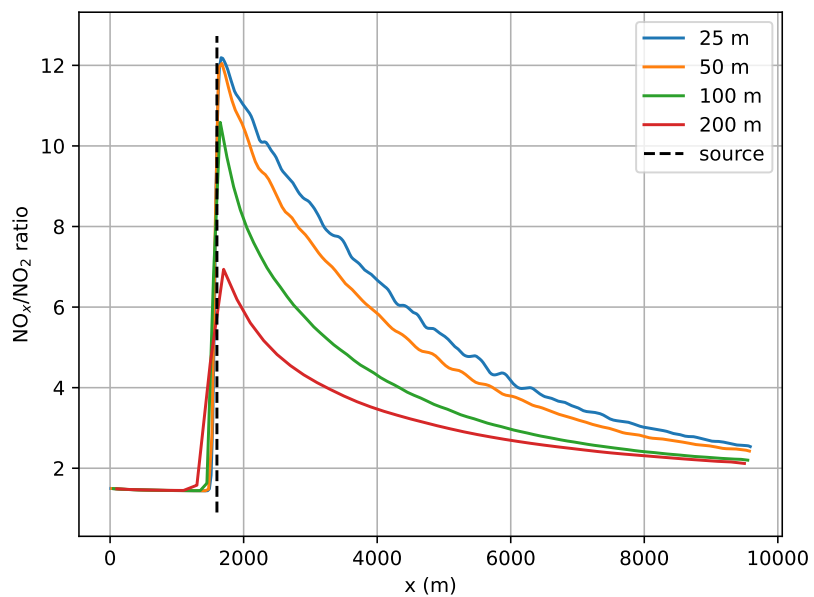
Figure S11. NO$_2$ y-mean columns from Fig. S10. The dotted line indicates the stack location.
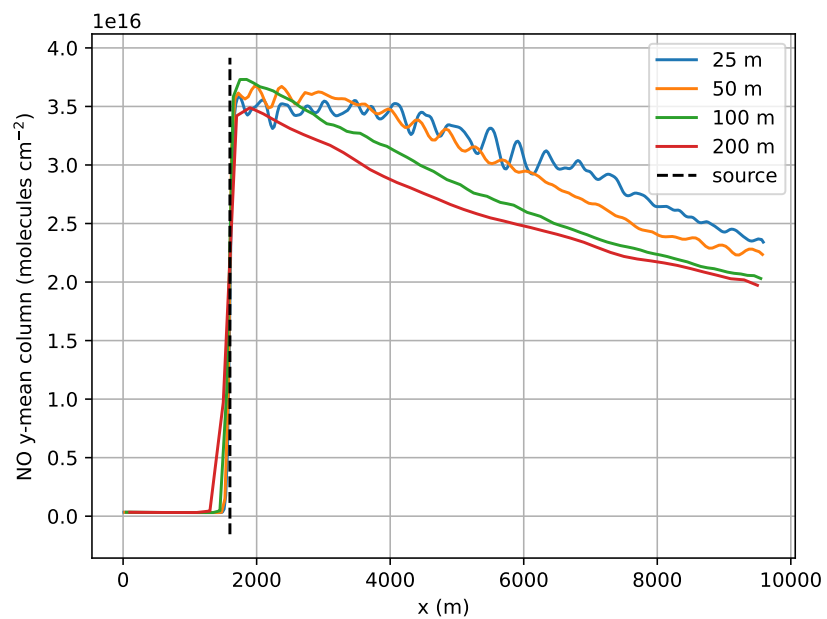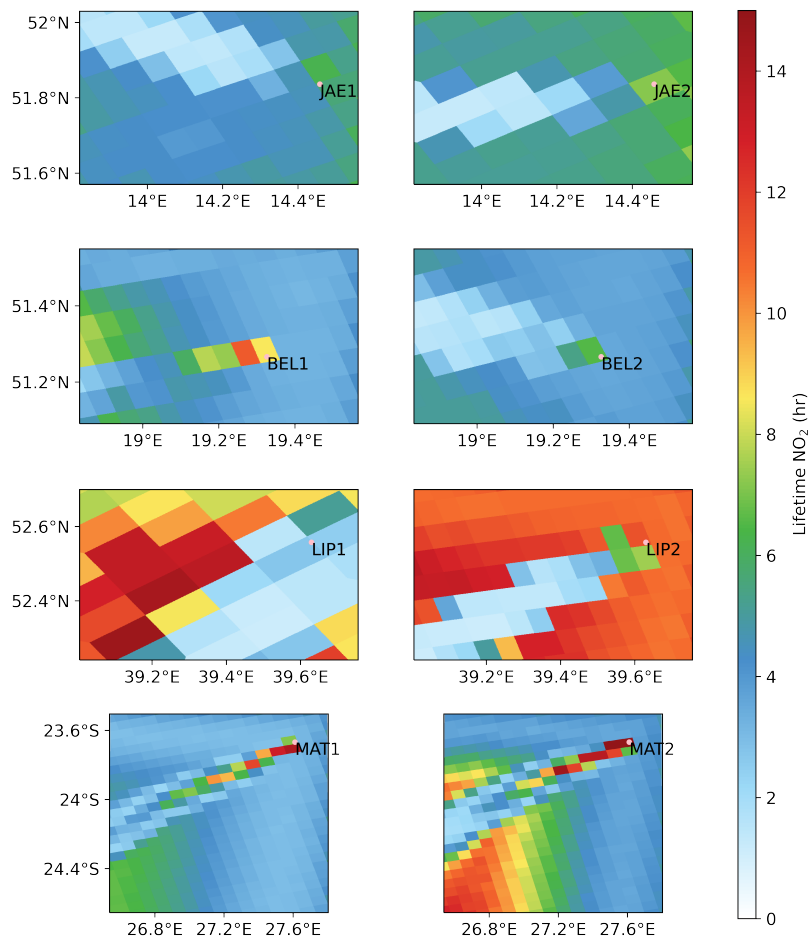

Figure S12. NO y-mean columns from Fig. S10. The dotted line indicates the stack location.
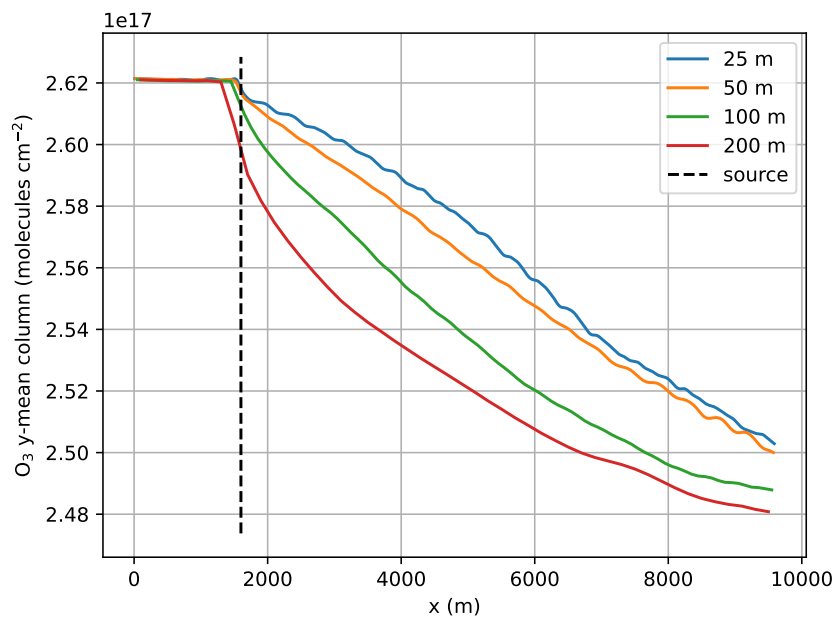
Figure S13. O_3 y-mean columns from Fig. S10. The dotted line indicates the stack location.

**Figure S14.** Y-mean NO_x over NO_2 ratio. The dotted line indicates the stack location.

10

Figure S15. NO$_2$ lifetime calculated over the entire domain and degraded to TROPOMI resolution. Values are calculated up to the height of the convective boundary layer. These boundary layer heights are respectively 2500 (JAE1), 2000 (JAE2), 1200 (BEL1), 1500 (BEL2), 1800 (LIP1), 1500 (LIP2), 1900 (MAT1), and 1850 m (MAT2).
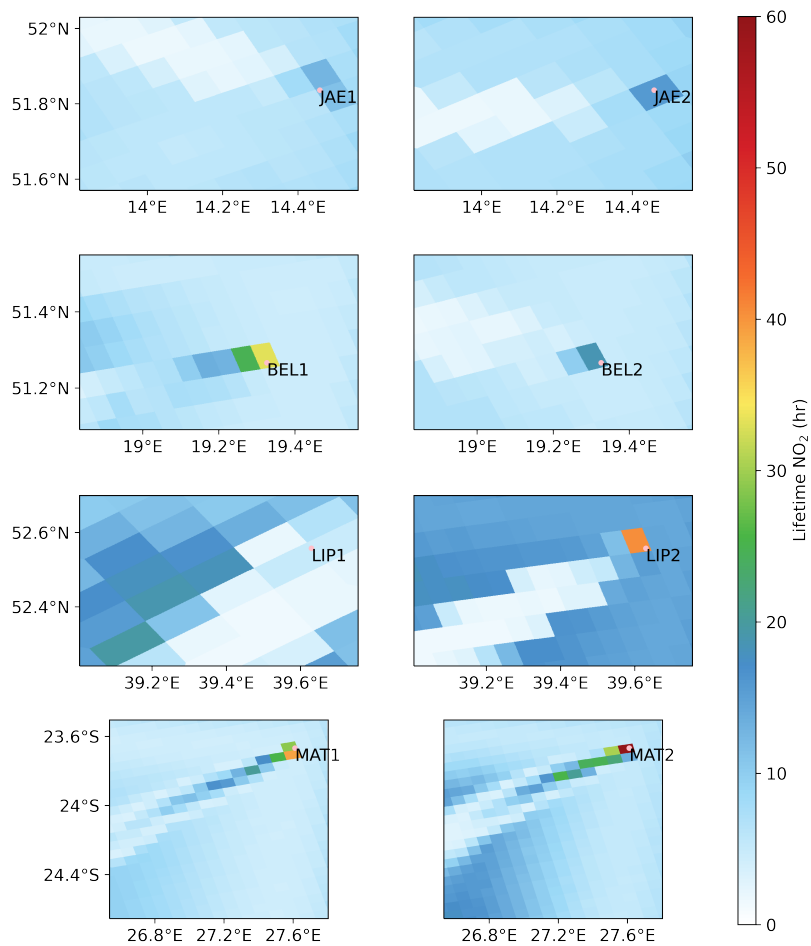
Figure S16. NO$_x$ lifetime calculated over the entire domain and degraded to TROPOMI resolution. Values are calculated up to the height of the convective boundary layer. These boundary layer heights are respectively 2500 (JAE1), 2000 (JAE2), 1200 (BEL1), 1500 (BEL2), 1800 (LIP1), 1500 (LIP2), 1900 (MAT1), and 1850 m (MAT2).
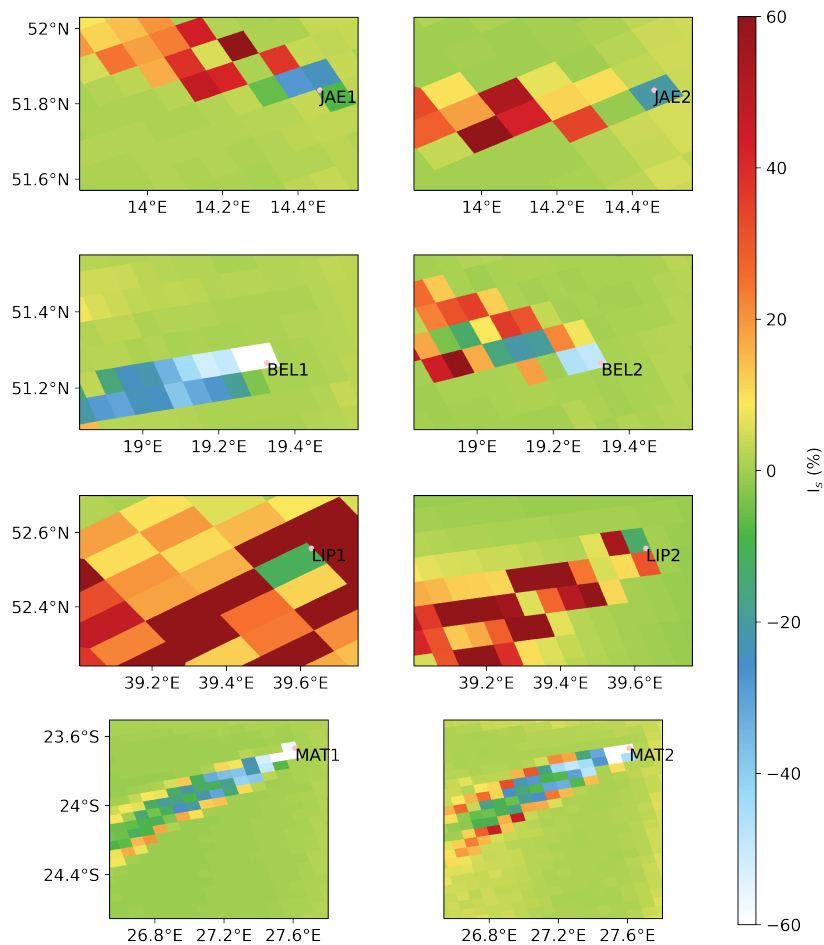
Figure S17. $I_{s,NO_2,OH}$ (in percent) calculated over the entire domain and degraded to TROPOMI resolution. Values are calculated up to the height of the convective boundary layer. These boundary layer heights are respectively 2500 (JAE1), 2000 (JAE2), 1200 (BEL1), 1500 (BEL2), 1800 (LIP1), 1500 (LIP2), 1900 (MAT1), and 1850 m (MAT2).
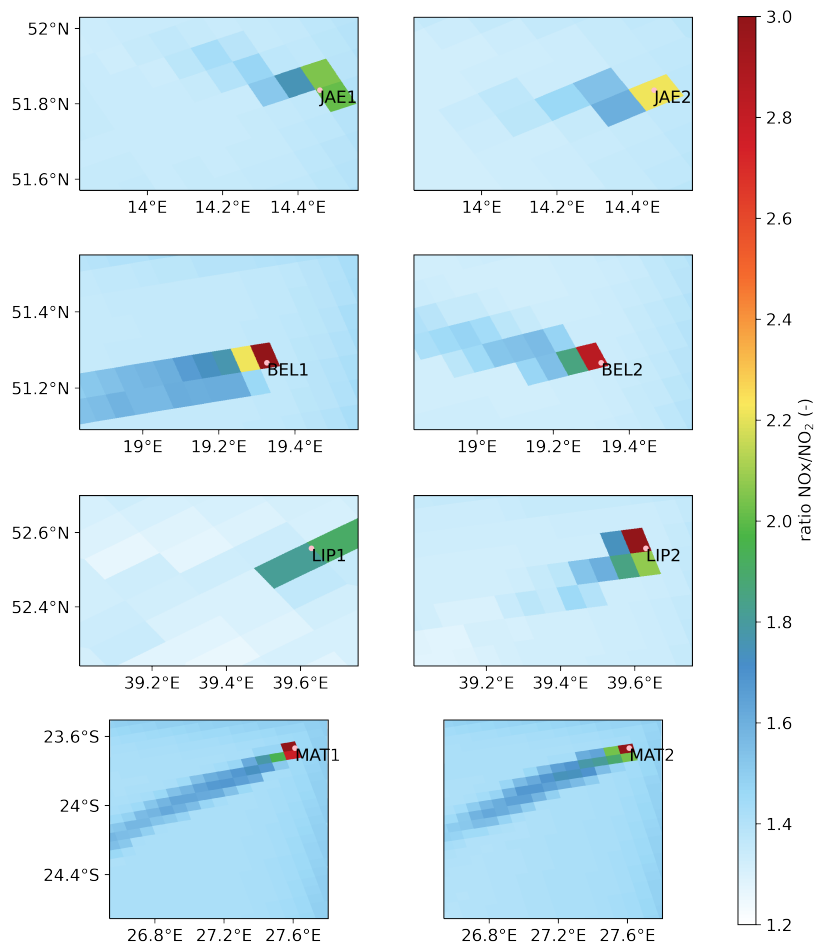
Figure S18. NO$_x$ to NO$_2$ ratio calculated over the entire domain and degraded to TROPOMI resolution. Values are calculated up to the height of the convective boundary layer. These boundary layer heights are respectively 2500 (JAE1), 2000 (JAE2), 1200 (BEL1), 1500 (BEL2), 1800 (LIP1), 1500 (LIP2), 1900 (MAT1), and 1850 m (MAT2).